Article:
Shaw, A.D., Neild, S.A. and Wagg, D.J. (2013) Dynamic analysis of high static low dynamic stiffness vibration isolation mounts. Journal of Sound and Vibration, 332 (6). 1437 - 1455. ISSN 0022-460X

https://doi.org/10.1016/j.jsv.2012.10.036

Dynamic Analysis of High Static Low Dynamic Stiffness Vibration Isolation Mounts

A. D. Shaw, S. A. Neild, D. J. Wagg

Advanced Composites Centre for Science and Innovation (ACCIS), University of Bristol, Queen's Building, Bristol, BS8 1TR, United Kingdom

Abstract

The High Static Low Dynamic Stiffness (HSLDS) concept is a design strategy for an anti-vibration mount that seeks to increase isolation by lowering the natural frequency of the mount, whilst maintaining the same static load bearing capacity. Previous studies have successfully analysed many features of the response by modelling the concept as a Duffing oscillator. This study extends the previous findings by characterising the HSLDS model in terms of two simple parameters. A fifth-order polynomial model allows us to explore the effects of these parameters. We analyse the steady state response, showing that simple changes to the shape of the force displacement curve can have large effects on the amplitude and frequency of peak response, and can even lead to unbounded response at certain levels of excitation. Harmonics of the fundamental response are also analysed, and it is shown that they are unlikely to pose significant design limitations. Predictions compare well to simulation results.

Keywords: Vibration Isolation, Nonlinear Dynamics, HSLDS, Normal form

1. Introduction

Vibration isolation is a vital requirement throughout much of engineering [1], particularly when there is a strong source of vibration such as a motor. It is frequently required to prevent the transmission of these vibrations to other elements of the system, for reasons such as passenger comfort in vehicles, or the protection of delicate electronic equipment.

One strategy for the isolation of vibration is to reduce the stiffness of a linear mount. A linear mass/spring/damper system has transmissibility that is less than unity at angular frequencies of $\omega > \sqrt{2k/m}$, where k is the stiffness of the mount and m is the mass being supported [1]. Reducing k will increase the size of the isolation region (it is assumed that increases in mass are undesirable). However, significantly reducing k may cause the mount to have an excessive static deflection on application of a static load [2] (this load typically consists of the weight of the mass). A further means of reducing vibration is to reduce the viscous damping coefficient, which dominates the response at high frequencies. However this has the disadvantage of increasing the peak transmissibility of response [1]; this will often be of concern, for example in the case of a motor where the mount is designed such that the motor's typical rotational velocity is within its isolation region, whenever the motor is started from rest it will pass through the natural frequency as it gains rotational speed.

A High Static Low Dynamic Stiffness (HSLDS) mount has a nonlinear force-displacement curve, which has decreased stiffness near the point of static equilibrium about which the mount oscillates, known as the dynamic stiffness. Elsewhere, the stiffness increases so that the static deflection due to its designed static load is reduced; in effect the mount shows high static stiffness [2]. A typical means of achieving this profile is by connecting a linear spring in parallel with an 'anti-spring' device [3], which is a mechanism that features a region of negative stiffness, discernible by a snap-through displacement response to static force.

Isolators that exhibit HSLDS behaviour have appeared in the literature, although the HSLDS term itself is relatively new. Winterflood [4] presents a mount utilising a Euler spring for use in gravitational experiments. Virgin and Davis [5] present a prototype mount consisting of a buckled strut, and Plaut et al. [6] present analysis of similar mount albeit with fixed as opposed to pinned end conditions. Virgin et al. [7] also propose a mechanism based on a strip bent into a tear-shaped loop. Further exposition and results for both these types of mount appear in Santillan's PhD thesis [8]. DeSalvo [9] presents a general

2

design deriving the required nonlinear response from a geometrical arrangement of springs, and presents results from an implementation using prestressed blade springs. Carrella et al. [10] presents analysis of a similar geometrical spring arrangement, with the aim of achieving near zero stiffness at equilibrium, known as Quasi Zero Stiffness (QZS). In a more recent paper, Carrella idealised the dynamic response of this mechanism as a Duffing oscillator, demonstrating important differences between its force transmissibility and motion transmissibility [11]. Kovacic et al. [12] also proposed oblique spring arrangements, but with nonlinear springs to reduce the variability in dynamic stiffness with displacement from equilibrium. Zhou, [13], has proposed an HSLDS using an electromagnetic negative spring element, that allows system parameters to be tuned. Robertson et al. [14] present theoretical analysis for a fully magnetic HSLDS device, where magnetism also supports the payload mass. Many HSLDS devices are found in a review of passive vibration isolation methods by Ibrahim [3]. Further designs, both magnetic and geometric, and more analysis of the nonlinear phenomena encountered by HSLDS mounts including amplitude dependant response and jump frequencies, based on Duffing oscillator models are given in [2]. In addition, Le and Ahn present analysis and an experimental prototype for a spring-based mechanism designed for isolation of a vehicle seat [15], showing that isolation is achieved for both broadband and harmonic signals.

The response of the HSLDS concept varies depending upon the form of excitation that the mount receives [11]. Furthermore, different aspects of the response may be considered important when evaluating the performance of the mount; for example the aim may be to reduce the displacement amplitude of the mass in some cases, whereas in others the aim may be to reduce the amplitude of the force transmitted to the base. Ideally, the nonlinearity in the mount will also have the effect of reducing the peak amplitude of response, because this can compensate for an increase in peak amplitude caused by reducing damping, and so allowing improved isolation at high frequencies. In this work, we consider the cases of displacement amplitude response to force excitation of the mass and displacement amplitude response to base motion excitation of the mount.

Regardless of the situation in which it is used, an HSLDS will only function usefully within limits of the response amplitude. As amplitude increases, the peak frequency of the mount increases reducing the isolation region [2], and harmonic responses increase, which could potentially negate reductions in response at forcing frequency. This paper extends previous work, by considering simple parameters that describe a generic HSLDS response, irrespective of its mechanism or the mathematical form of its force-displacement curve. We then show how these parameters affect HSLDS performance in terms of response amplitude, frequency and harmonics, using a 5th order model.

After the initial problem description, Section 2 defines a nondimensionalisation based on the static stiffness, that is intended to give clear insight into the effects of these system parameters. Section 3 analyses the HSLDS restoring force function in quasi-static terms, employing two parameters $\hat{k}_e$ and $\hat{x}_r$ that can be used to approximately characterise any HSLDS mount, including non-polynomial responses. We find that a 5th order polynomial system can exhibit a wide range of these parameters' values. In Section 4, we present a Normal Form analysis of the approximate steady-state dynamic response of HSLDS mounts to harmonic excitation [16, 17], including a useful graphical method and predictions for response harmonics. Section 6 compares analytical and numerical results for a range of systems, excited to amplitudes where highly nonlinear effects occur, showing that the analysis still provides reasonable results, and highlighting the important effects that different amplitude-frequency relationships can have on performance.

2. Idealisation of generic system

2.1. Equation of motion

Fig. (1) shows the idealised system to be considered; a mass m subject to static load F_s is supported by a nonlinear spring with force/displacement response $P_k(z)$ and linear damper with coefficient c on a base (Typically $F_s = mg$ due to the weight of the mass, although other static loads may be relevant).
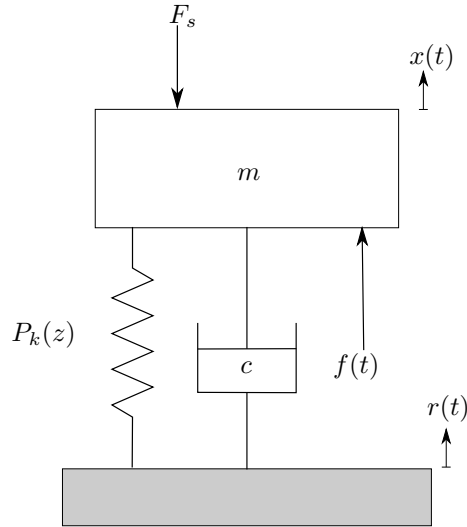
4

Figure 1: Mass m with static load F_s supported on movable base by nonlinear spring with linear damper with damping constant c. $r(t)$ denotes base motion, $x(t)$ denotes displacement response of the mass, $z \equiv x - r$ denotes relative displacement response, $f(t)$ denotes force excitation, nonlinear spring has force/displacement function $P_k(z)$.

It may be excited by forcing signal $f(t)$ or base excitation signal $r(t)$, resulting in an absolute displacement from the static equilibrium position x. This may also be expressed in terms of a relative displacement response given by:

$$z \equiv x - r \tag{1}$$

We specify that $z = 0$ at static equilibrium. The nonlinear spring will resist displacements from its static equilibrium position with a force $P(z) = F_s - P_k(z)$. Viscous damping force will also be determined by relative response, however inertial forces will be due to absolute acceleration $\ddot{x} = \ddot{r} + \ddot{z}$. Referring to Fig. (1), and substituting Eq. (1) for x, gives the following equation of motion:

$$m\ddot{z} + c\dot{z} + P(z) = f(t) + m\ddot{r} \tag{2}$$

2.2. Equivalent linear system

To assess the performance of the nonlinear mount, it is compared to a linear mount that has the same static deflection z_s when subjected to static load
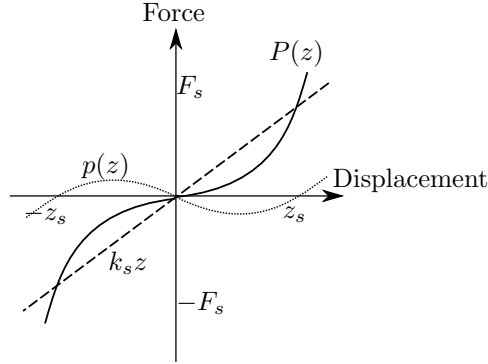
5

Figure 2: Relationship between different force/displacement functions used in analysis.

F_s. This linear mount, with equal damping coefficient c, is referred to as the equivalent linear system. It will have stiffness equal to the static stiffness of the system given by $k_s \equiv F_s/z_s$. It is often useful to consider the distortions of the nonlinear force-deflection function from those of the equivalent linear mount, hence we define:

$$p(z) \equiv P(z) - k_s z \tag{3}$$

It is assumed that this distortion is odd about the static equilibrium $z = 0$, hence $p(\pm z_s) = 0$. The relationship between $P(z)$, $p(z)$ and the linear restoring function $k_s z$ are illustrated in Fig. (2).

2.3. Nondimensionalisation of system

Recalling that static load bearing and static displacement are key to the motivation for an HSLDS, we treat them as design constraints, and therefore nondimensionalise forces by F_s and displacements by z_s. Using $\omega_e \equiv \sqrt{k_s/m}$, $\lambda \equiv c/(2\sqrt{k_s m})$, $\hat{r} \equiv r/z_s$, $\hat{z} \equiv z/z_s$ and substituting Eq. (3) into Eq. (2) gives:

$$\ddot{\hat{z}} + 2\lambda\omega_e\dot{\hat{z}} + \omega_e^2\hat{z} + \frac{p(\hat{z}z_s)}{mz_s} = \frac{f(t)}{mz_s} + \ddot{\hat{r}} \tag{4}$$

Note that ω_e is the natural frequency of the equivalent linear system, not the more commonly seen ω_n which is the natural frequency of the linearised system which is used later on. Similarly λ is used instead of the usual damping ratio ζ because it is nondimensionalised by static stiffness, not linearised stiffness. In

6

this way, our damping is not affected by changes to stiffness nonlinearities. We can also scale time by the natural frequency of the equivalent linear system by defining:

$$\tau \equiv t\omega_e \tag{5}$$

If the prime $\prime$ is now used to denote differentiation w.r.t τ, we can write:

$$\hat{z}'' + 2\lambda\hat{z}' + \hat{z} + \hat{p}(\hat{z}) = \hat{f}(\tau) + \hat{r}'' \tag{6}$$

where $\hat{p}(\hat{z}) \equiv \frac{p(\hat{z}z_s)}{F_s}$ and $\hat{f}(\tau) \equiv \frac{f(t/\omega_e)}{F_s}$. We can also create a nondimensional form of the original $P(z)$:

$$\hat{P}(\hat{z}) \equiv \frac{P(\hat{z}z_s)}{F_s} = \hat{p}(\hat{z}) + \hat{z} \tag{7}$$

such that $\hat{P}(1) = 1$. For completeness, we also define a nondimensionalised absolute response $\hat{x} = x/z_s$.

We can see that results occurring for the nondimensional system can be applied to any dimensional system by simple scaling operations. Note that nondimensional displacements of unity are equal in magnitude to the static displacement.

3. Nonlinear force displacement response

3.1. General characteristics of HSLDS force-displacement response

We propose two parameters that give a good overall characterisation of the response. The first is equilibrium stiffness $\hat{k}_e$, defined as the non-dimensional stiffness at the equilibrium point:

$$\hat{k}_e \equiv \left. \frac{d\hat{P}}{d\hat{z}} \right|_{\hat{z}=0} \tag{8}$$

This will have a value between zero and one, with one indicating no softening effect relative to the equivalent linear system. The second parameter is the reduced stiffness range $\hat{z}_r$. This is the range of displacement over which the stiffness is less than that of the equivalent linear system:

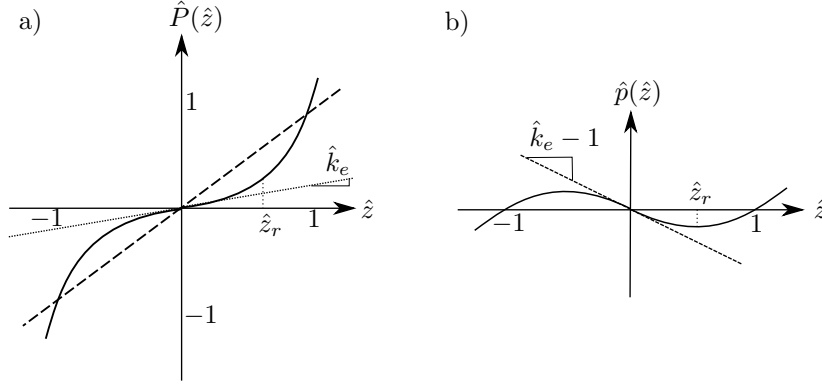$$\left. \frac{d\hat{P}}{d\hat{z}} \right|_{|\hat{z}|<\hat{z}_r} < 1 \tag{9}$$

7

Figure 3: Illustration of properties $\hat{z}_r$ and $\hat{k}_e$. (a) Nondimensional force displacement function $\hat{P}(\hat{z})$ (solid) showing equilibrium stiffness $\hat{k}_e$ (fine dash) and nondimensional equivalent linear system (large dash) (b) Nondimensional distortions from equivalent linear response $\hat{p}(\hat{z})$ (solid) with zero gradient (dashed)

Therefore a system with a greater $\hat{z}_r$ will retain low dynamic stiffness over a greater range of displacement relative to its static deflection. Fig. (3) illustrates these properties in relation to $\hat{P}(\hat{z})$ and $\hat{p}(\hat{z})$. We find $\hat{z}_r$ by considering the minimum of $\hat{p}(\hat{z})$ i.e. by solving:

$$\frac{d\hat{p}}{d\hat{z}}\bigg|_{\hat{z}=\hat{z}_r} = 0 \ , \ \frac{d^2\hat{p}}{d\hat{z}^2}\bigg|_{\hat{z}=\hat{z}_r} > 0 \tag{10}$$

We would like the shape of the designed response to be relatively simple so we place some additional restrictions upon it. Firstly we stipulate that the minimum stiffness is located at the equilibrium point ($\hat{z} = 0$), expressed mathematically as:

$$\frac{d^2\hat{P}}{d\hat{z}^2}\bigg|_{\hat{z}=0} = 0 \ , \ \frac{d^3\hat{P}}{d\hat{z}^3}\bigg|_{\hat{z}\to 0} > 0 \tag{11}$$

with the first part of this automatically satisfied by the use of an odd function for $\hat{p}(\hat{z})$. Secondly we stipulate that there are no positive regions of $\hat{p}(\hat{z})$ between zero and one (hence no roots of $\hat{p}(\hat{z})$ in this region); this implies that the magnitude of restoring force is always less than that of the equivalent linear system when $|\hat{z}| < 1$. For completeness, we reiterate that $\hat{P}(\hat{z})$ is an odd function such that:

$$\hat{P}(1) = 1 \tag{12}$$

8

3.2. Constrained 5th order polynomial form

Polynomial response forms are of interest because they may be used to approximate many other functions. We use a 5th order polynomial, to allow greater variation in response than a 3rd order polynomial. We require $\hat{P}(\hat{x})$ to be odd, so only the odd powers are included in the polynomial. The fifth order function is therefore given as:

$$\hat{P}(\hat{z}) = k_1\hat{z} + k_3\hat{z}^3 + k_5\hat{z}^5 \tag{13}$$

We satisfy Eq. (8) by setting $k_1 = \hat{k}_e$. We choose the other coefficients by substituting Eq. (13) into the first part of Eq. (10) and Eq. (12) and solving to get:

$$k_3 = (1 - \hat{k}_e)\frac{5\hat{z}_r^4 - 1}{5\hat{z}_r^4 - 3\hat{z}_r^2} \tag{14}$$

$$k_5 = (1 - \hat{k}_e)\frac{1 - 3\hat{z}_r^2}{5\hat{z}_r^4 - 3\hat{z}_r^2} \tag{15}$$

Our choice of $\hat{z}_r$ is constrained; we find that to satisfy Eq. (11) and ensure no roots of $\hat{p}(\hat{z})$ less than one, we require that $\sqrt{1/5} \le \hat{z}_r \le \sqrt[4]{1/5}$. We find that at these limiting values of $\hat{z}_r$, we can obtain simpler formulas for k_3 and k_5:

$$k_{3_{(\hat{z}_r = \sqrt{1/5})}} = 2(1 - \hat{k}_e) \ , \ k_{5_{(\hat{z}_r = \sqrt{1/5})}} = \hat{k}_e - 1 \tag{16}$$

$$k_{3_{(\hat{z}_r = \sqrt[4]{1/5})}} = 0 \ , \ k_{5_{(\hat{z}_r = \sqrt[4]{1/5})}} = 1 - \hat{k}_e \tag{17}$$

Furthermore, we note that by choosing $\hat{z}_r = \sqrt{1/3}$ we obtain:

$$k_{3_{(\hat{z}_r = \sqrt{1/3})}} = 1 - \hat{k}_e \ , \ k_{5_{(\hat{z}_r = \sqrt{1/3})}} = 0 \tag{18}$$

which is the Duffing oscillator. Also note that the expression for minimal x_r gives k_3 as twice that of the Duffing oscillator, and that the expression for maximal $\hat{z}_r$ gives a purely 5th order response. Fig. (4) shows the range of response profiles achievable with the constrained 5th order polynomial (parts (a) to (c)), and examples of choosing $\hat{z}_r$ outside the appropriate limits (parts (d) and (e)). Despite the constraints, we see that the 5th order form allows significant exploration of the effects of these parameters.
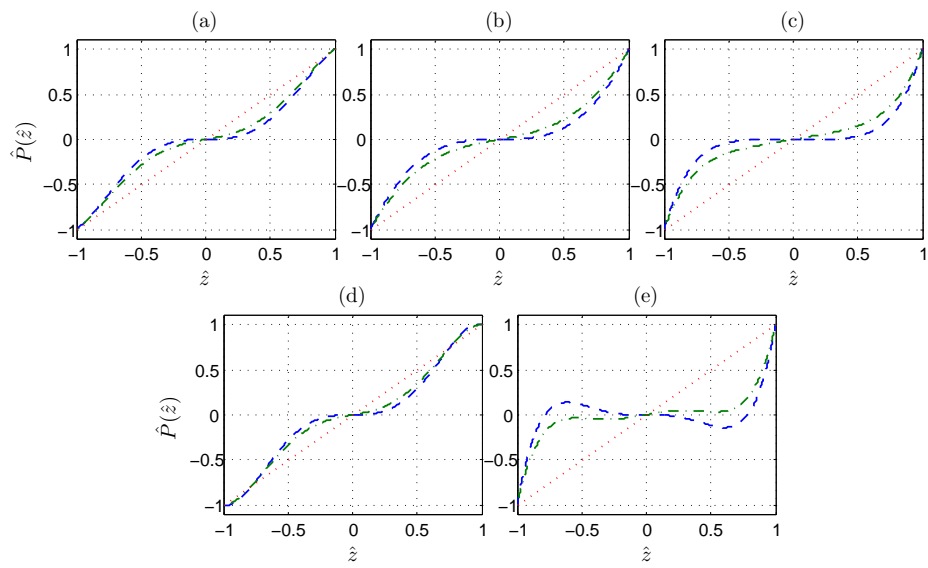
9

Figure 4: Effect of $\hat{z}_r$ on 5th order polynomial response profile. (a) $\hat{z}_r = \sqrt{1/5}$ (b) $\hat{z}_r = \sqrt{1/3}$ (Duffing response) (c) $\hat{z}_r = \sqrt[4]{1/5}$ (d) Effect of $\hat{z}_r < \sqrt{1/5}$, which gives positive regions of $\hat{p}(\hat{z})$ between zero and one (e) Effect of $\hat{z}_r > \sqrt[4]{1/5}$ which fails to meet Eq. (11) and can show regions of negative stiffness. Dashed line: $\hat{k}_e = 0.01$ Dot-dashed line: $\hat{k}_e = 0.25$. Dotted line: $\hat{k}_e = 1$ (Equivalent linear system).

3.3. Comparison to real HSLDS mechanisms

Fig. (5) gives an example of this nondimensionalisation fitted to a non-polynomial response, given by a system using a vertical spring coupled to pre-compressed lateral springs to provide geometric nonlinearity, analysed by Car-rella [11]. This response is given by:

$$P(z) = k_v z + 2k_h (1 - \frac{\ell_0}{\sqrt{z^2 + \ell^2}})z \tag{19}$$

where k_v and k_h are the vertical and lateral spring constants respectively, and ℓ_0 and ℓ are the original and compressed lengths of the horizontal springs. The left hand graph shows this response with $k_v = k_h = 10$ N mm^{-1}, $\ell_0 = 10$ mm, and $\ell = 7$ mm. If we assume that static load $F_s = 150$N, implying static displacement $z_s = 10.6$mm, Eq. (8) gives $\hat{k}_e = 0.101$ and $\hat{z}_r = 0.462$. The right hand graph shows the effect of nondimensionalising this system, along with a Duffing approximation that matches $\hat{k}_e$, and a 5th order function that matches both $\hat{k}_e$ and $\hat{z}_r$. It can be seen that the constrained 5th order response follows the original function more accurately than the Duffing over the range of fitting.

4. Normal form analysis of polynomial HSLDS

A Normal Form analysis is used, based on the technique described by Neild and Wagg [16, 17], which provides results in terms of a transformed variable $\hat{u}$ representing the response at the forcing frequency, and a transformation function $h(\hat{u})$ which contain information on harmonic responses. A slight modification to the method is made to improve accuracy of harmonics at forcing frequencies below resonance; the full derivation is supplied in Appendix A, whilst the main results are shown here.

4.1. Fundamental response solution

To solve Eq. (6) we transform $\hat{r}$ as follows:
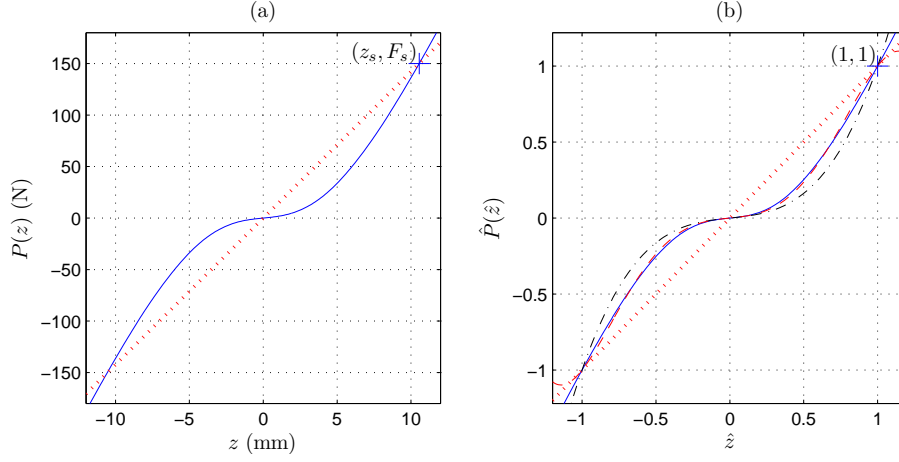
$$\hat{u} = \hat{z} - h(\hat{u}) \tag{20}$$

Figure 5: (a) Solid line shows response of oblique spring HSLDS mount with $k_v = k_h = 10$ N mm^{-1}, $\ell_0 = 10$ mm, $\ell = 7$ mm. Red dots show linear mount implied by chosen static load $F_s = 150$ N, giving static displacement $x_s = 10.6$ mm. (b) Consequent nondimensionalisation to $\hat{P}(\hat{z})$ (solid) with Duffing (dot-dashed) and 5th order (dashed) models fitted, $\hat{k}_e = 0.101$, $\hat{z}_r = 0.462$.

where $\hat{u}$ represents the displacement response at forcing frequency and $h(\hat{u})$ is a near identity transformation that effectively represents harmonic responses. The Normal Form analysis allows the definition of response functions relating fundamental response amplitude $\hat{U}$, harmonic excitation amplitude and fundamental response angular frequency $\hat{\omega}_r$. For base excitation the equation that must be solved is :

$$\hat{\omega}_r^4(\hat{U}^2 - \hat{R}^2) + 2\hat{\omega}_r^2\hat{U}^2\left[2\lambda^2 - K(\hat{U})\right] + K(\hat{U})^2\hat{U}^2 = 0 \qquad (21)$$

where $\hat{R}$ is the amplitude of base excitation, whereas for forced excitation the response function is:

$$\hat{\omega}_r^4\hat{U}^2 + 2\hat{\omega}_r^2\hat{U}^2\left[2\lambda^2 - K(\hat{U})\right] + K(\hat{U})^2\hat{U}^2 - \hat{F}^2 = 0 \qquad (22)$$

where $\hat{F}$ is the amplitude of forcing. These may be solved for $\hat{\omega}_r^2$ with any trial value of response amplitude at forcing frequency $\hat{U}$, yielding up to 2 real solutions. $K(\hat{U})$ represents amplitude dependant stiffness and for a 5th order

12

polynomial is:

$$K(\hat{U}) = \hat{k}_e + \frac{3k_3\hat{U}^2}{4} + \frac{10k_5\hat{U}^4}{16} \tag{23}$$

4.2. Backbone and limit curves

A curve along which all solutions of peak fundamental response amplitude and the excitation frequencies at which they occur, known as the backbone curve [18], may be obtained for both base motion and forced excitation as:

$$\hat{\omega}_r = \sqrt{K(\hat{U})} \tag{24}$$

There is also a relationship between response amplitude, forcing frequency, forcing amplitude and damping that applies to all systems when at peak amplitude, regardless of stiffness function, known as the limit curve [18]. For base motion excitation it is:

$$\hat{U} = \frac{\hat{\Omega}\hat{R}}{2\lambda} \tag{25}$$

whereas for forcing excitation it is:

$$\hat{U} = \frac{\hat{F}}{2\lambda\hat{\Omega}} \tag{26}$$

We note that in the base excitation case, peak amplitude is proportional to peak forcing frequency, whereas for forced excitation it is inversely proportional.

4.3. Absolute response

For base excitation it is often necessary to know the absolute displacement response in addition to the relative displacement response. In this case it is necessary to know the phase difference between the base excitation and the response, given by:

$$\phi = \cos^{-1}\left(\frac{-\hat{\omega}_r^2\hat{U} + K(\hat{U})\hat{U}}{\hat{\omega}_r^2\hat{R}}\right) \tag{27}$$

We can then calculate $\hat{X}$, the amplitude of absolute response at the forcing frequency, as:

$$\hat{X} = \sqrt{(\hat{U} + \hat{R}\cos(\phi))^2 + (\hat{R}\sin(\phi))^2} \tag{28}$$

13

4.4. Estimation of Harmonics

This process is the same for both forced and base motion excitation, and is shown in more detail in Appendix A.3. We use the magnitude of the fundamental response $\hat{U}$ to find the magnitude of the 3rd and 5th harmonics using:

$$h_3(\hat{U}) = \left(\frac{k_3 \hat{U}^3}{4} + \frac{5 k_5 \hat{U}^5}{16} \right) \frac{1}{\sqrt{(9\hat{\omega}_r^2 - \hat{\omega}_n^2)^2 + (6\hat{\omega}_r \lambda)^2}} \tag{29}$$

and

$$h_5(\hat{U}) = \frac{k_5 \hat{U}^5}{16} \frac{1}{\sqrt{(25\hat{\omega}_r^2 - \hat{\omega}_n^2)^2 + (10\hat{\omega}_r \lambda)^2}} \tag{30}$$

where $\hat{\omega}_n^2 = \hat{k}_e$.

5. Backbone and limit curve maps

In Section 4.2 we saw that when the back bone curve, as given by Equation (24), intersects a limit curve, given by either Eq. (25) for base motion excitation or Eq. (26) for forced excitation, a solution for peak response occurs. We also noted that limit curves were independent of the stiffness properties of the mount.

In this section we display this graphically to gain insight into the effects of the system parameters. We plot limit curves for a range of excitation amplitudes and damping levels, then superimpose backbone curves for a range of nonlinear springs upon them. These diagrams therefore constitute a 'map' showing the peak response for any combination of backbone curve, excitation amplitude and damping; to find a peak response, simply inspect where the backbone curve concerned intersects the relevant limit curve.

The systems presented here have equilibrium stiffnesses k_e of 0.25 and 0.01 (recalling that linearised natural frequency is proportional to the square root of stiffness, we see that these lead to reductions in the linearised natural frequency to one half and one tenth of that of the equivalent linear system respectively). Referring to Fig. (4), we show $\hat{z}_r$ values of 0.447, 0.577 and 0.669 representing the minimal, Duffing and maximal values respectively for each stiffness.

From Eqs. (23) and (24), we see that all back bone curves cut the $\hat{\omega}_r$ axis at $\hat{\omega}_r = \sqrt{k_e}$, regardless of choice of $\hat{z}_r$. This is the nondimensional peak frequency
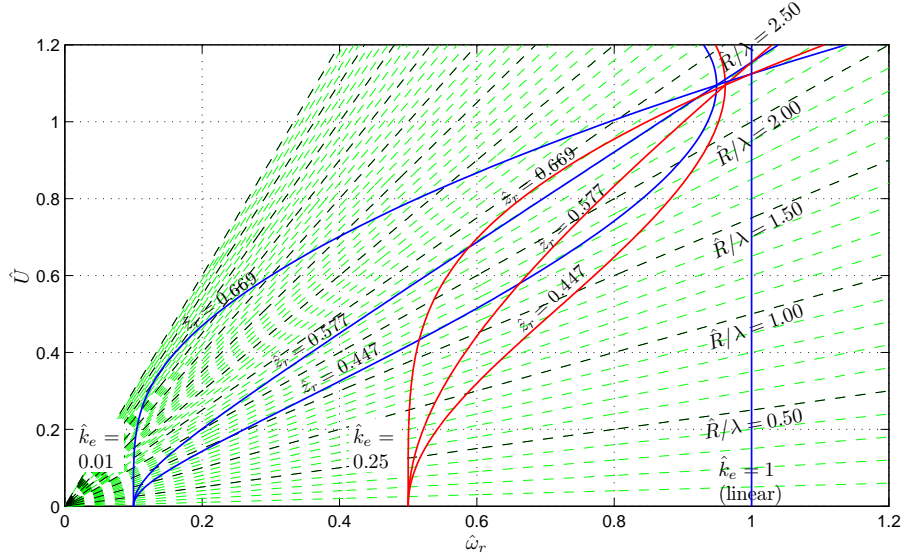
14
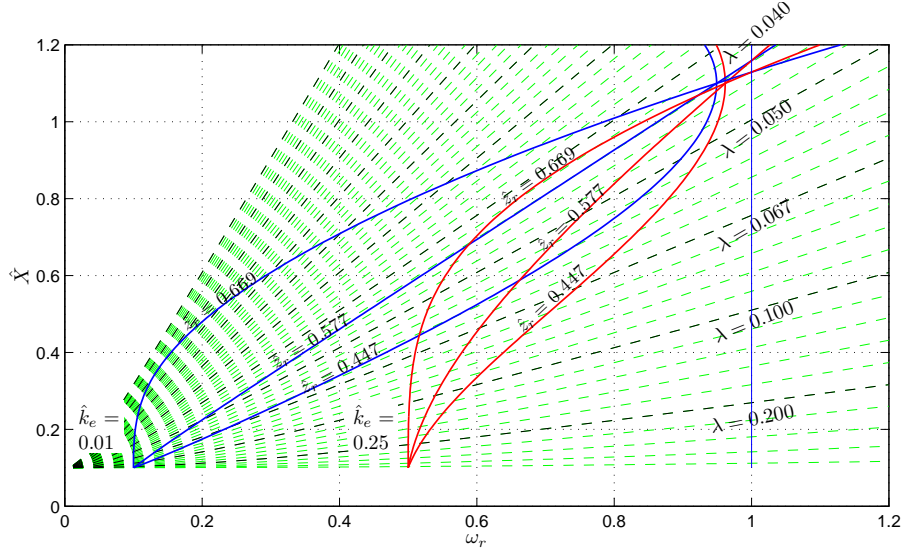
Figure 6: Limit (dashed) and backbone (solid) curves for resonant relative displacement response to harmonic base excitation.

predicted by linearised analysis, due to nonlinear polynomial terms becoming insignificant as amplitude tends to zero. Hence at small amplitude, $\hat{k}_e$ dominates response. However, as amplitude increases, the curves take different shapes depending on $\hat{z}_r$, leading to the different responses as described in the following sections.

5.1. Base Motion Excitation

We see from Fig. (6) that under base excitation with any given excitation amplitude and damping, a backbone that achieves a lower peak frequency will also achieve a lower peak amplitude, because all limit curves are straight lines from the origin. This effect occurs regardless of whether the peak frequency reduction is due to changes in equilibrium stiffness or reduced stiffness range, and is highly beneficial as it means that both peak frequency and peak amplitude reduction are achieved.

However, as excitation amplitude increases, the differences due purely to

Figure 7: Limit (dashed) and backbone (solid) curves for resonant absolute displacement response to harmonic base excitation. $\hat{R} = 0.1$

the shape of the backbone curve become dramatic. If we consider the line $\hat{R}/\lambda = 2.00$, and equilibrium stiffness $\hat{k}_e = 0.01$, choosing $\hat{z}_r = 0.447$ leads to a far greater peak amplitude and frequency than $\hat{z}_r = 0.577$ or $\hat{z}_r = 0.669$. This pattern is repeated for $\hat{k}_e = 0.25$, albeit less dramatically.

We note that in several places, the backbone curves run almost parallel to adjacent limit curves. For example when $\hat{k}_e = 0.01$, the $\hat{z}_r = 0.447$ backbone curve is almost parallel to the limit curve for $\hat{R}/\lambda = 2.00$ and other adjacent limit curves for $0.3 < \hat{\omega}_r < 0.8$. This implies that systems in this region are highly sensitive to changes in parameters, because a small increase in excitation (or reduction in damping) will lead to a large increase in frequency and amplitude before the backbone and limit curves intersect. Indeed, we have already seen how the $\hat{k}_r = 0.447$ back bone curve has a far greater peak amplitude and frequency than the other choices of $\hat{z}_r$ when $\hat{k}_e = 0.01$.

We note from the values of the ratio $\hat{R}/\lambda$ in Fig. (6) that $\hat{R}$ must be of a similar order of magnitude to λ, and therefore small due to our assumption

16

of light damping. Therefore, in the cases shown here there is no possibility of secondary resonances occurring, as these require hard excitation [19].

Fig. (6) also suggests the possibility of unbounded response; the backbone curve for $\hat{k}_e = 0.25$ and $\hat{z}_r = 0.669$ never intersects the limit curve for $\hat{R}/\lambda = 2.5$. This situation is clearly undesirable for an isolator, as there is no isolation region. This response is similar to the analytical prediction of unbounded motion transmissibility for a Duffing oscillator made by Carrella in [11]

We note that all curves intersect the limit line $\hat{Z}/\lambda = 2.00$, hence for this level of excitation or less there is no risk of unbounded response, and peak frequency and amplitude will both be reduced by the HSLDS mount relative to the equivalent linear system in all cases shown.

For absolute response, we recall that at resonance phase $\phi = \pi/2$, hence Eq. (28) becomes:

$$\hat{X} = \sqrt{\hat{U}^2 + \hat{R}^2} \tag{31}$$

We use this result to transform Fig. (6) for any given value of $\hat{R}$; this has been done in Fig. (7) for $\hat{R} = 0.1$. We note that absolute displacement response cannot be less than $\hat{R}$ at resonance, but as the relative response increases due to decreasing damping ratio, $\hat{U}$ becomes dominant over $\hat{R}$, and the upper half of Fig. (7) is highly similar to Fig. (6). We see that the base motion amplitude dominates when the damping is relatively high ($\lambda > 0.2$), or for low frequencies for backbone curves that have very low $\hat{k}_e$. The former case is unlikely to be relevant, because as discussed previously we seek light damping to reduce high frequency response. The latter case merely reflects that a mount with very low $\hat{k}_e$ reduces the resonant relative response so that it is much smaller than the excitation amplitude. Note also that as the excitation amplitude gets smaller, Fig. (7) becomes increasingly similar to Fig. (6) as the minimum $\hat{X}$ value reduces.

Finally, we emphasise the importance that the shape of the backbone curve has on response; we have demonstrated significant differences in response for systems with identical static stiffness and identical equilibrium stiffness.

17

5.2. Forcing Excitation

Fig. (8) shows that the forcing case will have a significantly different character to the base motion excitation case shown in Fig. (6), due to the different shape of the limit curves. Firstly, we see that for any given forcing excitation amplitude and damping, denoted by a single limit curve, a reduction in peak frequency will always be accompanied by an increase in peak amplitude, causing a trade off between frequency reduction and peak amplitude if the displacement response is of concern. This effect is greater where the limit curves are steeper; we see that further frequency reduction for the mount with $k_e = 0.01$ would lead to dramatic increases in peak amplitude. (Note that the increase in peak displacement response does not necessarily imply increased peak force transmission to the base—Carrella has shown that an HSLDS mount can reduce both peak frequency and amplitude for force transmissibility [2]).

We note from the values of the ratio $\hat{F}/\lambda$ in Fig. (8) that $\hat{F}$ must be of a similar order of magnitude to λ, and therefore small due to our assumption of light damping. Therefore, in the cases shown here there is no possibility of secondary resonances occurring, as these require hard forcing [19].

We notice that there is no danger of a backbone curve running parallel to a limit curve causing high parameter sensitivity, as seen for the base motion excitation case in Section 5.1. In addition, there is no danger of unbounded response.

6. Results and Comparison to Simulation

Sections 6.2 and 6.1 show the predicted and simulated frequency responses of a range of 5th order polynomial systems subject to forcing and base motion excitation respectively. Section 6.3 then presents a comparison of predicted and simulated results for the non-polynomial response function described in Section 3.3.

Markers show the results of simulations of forced response and absolute displacement response plots. The solver used is a Newmark scheme, with the

18
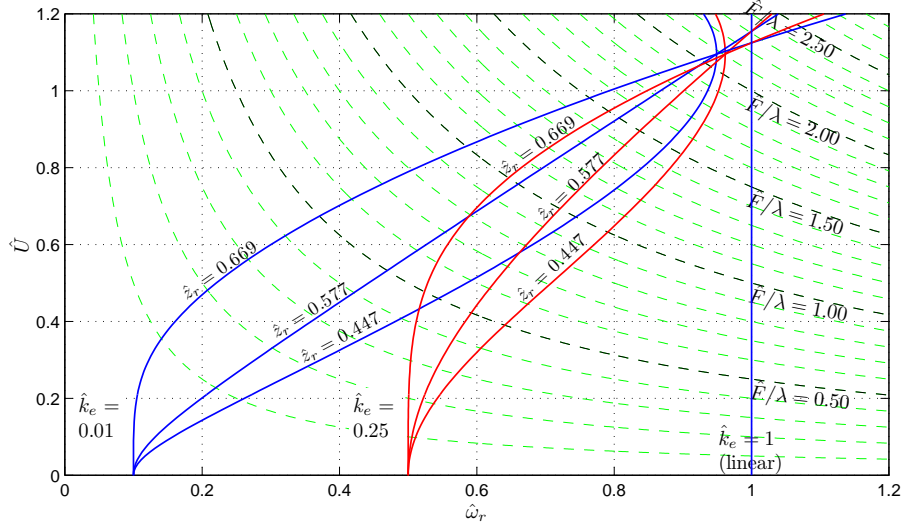
Figure 8: Limit (dashed) and backbone (solid) curves for resonant displacement response to harmonic forcing excitation.

sampling frequency set to 100 times per forcing period. The scheme steps both upwards ($*$) and downwards ($\circ$) through the frequency range to ensure each side of the nonlinear peak is captured. 100 forcing cycles are completed at each frequency, with the final cycle used for the calculation of Fourier series terms for the calculation of fundamental and harmonic responses.

6.1. Base Motion Excitation Frequency Response Functions

Fig. (9) to Fig. (11) show that the predictions of Sections 4.1 and 4.2 show close agreement with simulation, with some differences becoming visible in Fig. (11) as the response amplitude becomes large. The case of unbounded response discussed in Section 4.2 is also clearly reproduced.

Fig. (9) and Fig. (10) show that increasing $\hat{z}_r$ reduces both the frequency and amplitude of the peak response, and that the base motion case is highly sensitive to this parameter. We also see that reducing $\hat{k}_e$ gives significant benefit in terms of both peak frequency and peak amplitude, except in the case where

19

$\hat{z}_r = 0.447$, where both choices of $\hat{k}_e$ give an approximately similar peak response that is close to that of the equivalent linear system.

In Fig. (11) we increase the base motion amplitude further, and see that the lowest $\hat{z}_r$ has the lowest peak amplitude and frequency, $\hat{z}_r = 0.577$ has a peak response that exceeds the equivalent linear system in both frequency and amplitude, and the highest $\hat{z}_r$ has a peak response that is seemingly unbounded in both frequency and amplitude.

We see from Fig. (12) and Fig. (13) that the magnitudes of harmonic responses are at least an order of magnitude below that of the fundamental in the cases shown, suggesting that harmonics are unlikely to be limiting design issues. Fig. (12) and Fig. (13) show that predictions are reasonable for the third harmonic. Accuracy of the 5th harmonic magnitude is poor in both cases when $\hat{z}_r = 0.447$. This is because the Normal Form method effectively sums the contributions of different polynomial terms, as if they were linear terms which could be combined by superposition. The error that this introduces is clearly significant in relation to the size of the 5th harmonic. Referring to Eq. (16) to Eq. (18), we see that the case when $\hat{z}_r = 0.447$ is the only case where both k_3 and k_5 are nonzero, hence this is the only case afflicted by this problem.

6.2. Forced Excitation Frequency Response Functions

In the case of forced excitation, we see similar agreement between Fig. (8) and simulated results, confirming that peak frequency reduction is gained at the expense of increased peak amplitude.

6.3. Approximation of non-polynomial HSLDS response

Finally, Fig. (14) (a) shows simulated results for the non-polynomial HSLDS system shown in Fig. (5), superimposed on a Normal Form prediction for the 5th order polynomial approximation that matches $\hat{k}_e$ and $\hat{z}_r$ as described in Section 3.2. We see generally good agreement between the Normal Form prediction for the 5th order polynomial and the non-polynomial simulation. Fig. (14) (b) shows how a limit curve map could be used to consider changes to the

20
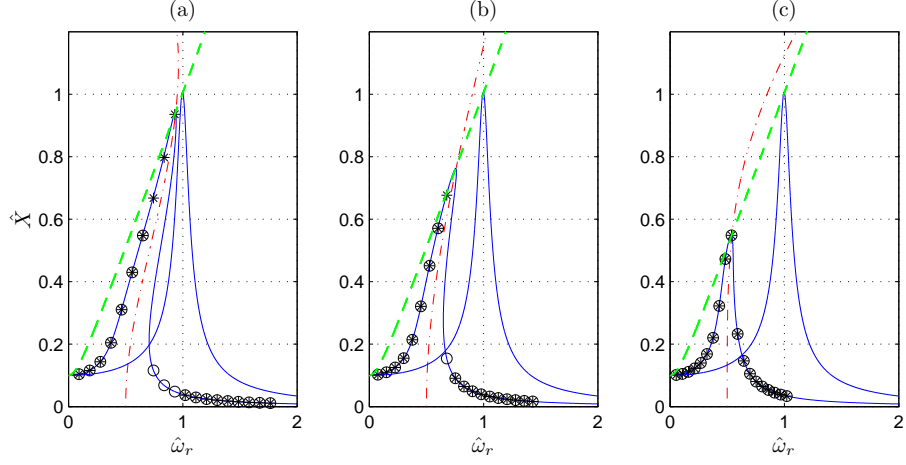
Figure 9: Predicted displacement FRF at forcing frequency for base motion excitation (solid) (a) $\hat{z}_r = 0.447$ (b) $\hat{z}_r = 0.577$ (c) $\hat{z}_r = 0.669$. Right hand peak shows response of equivalent linear system for comparison. Markers show simulation results; ($*$) denotes upwards frequency stepping, ($\circ$) denotes downwards frequency stepping. Dashed line shows limit curve, dot-dashed line shows backbone curve. $\hat{k}_e = 0.25$, $\lambda = 0.05$, $\hat{R} = 0.1$
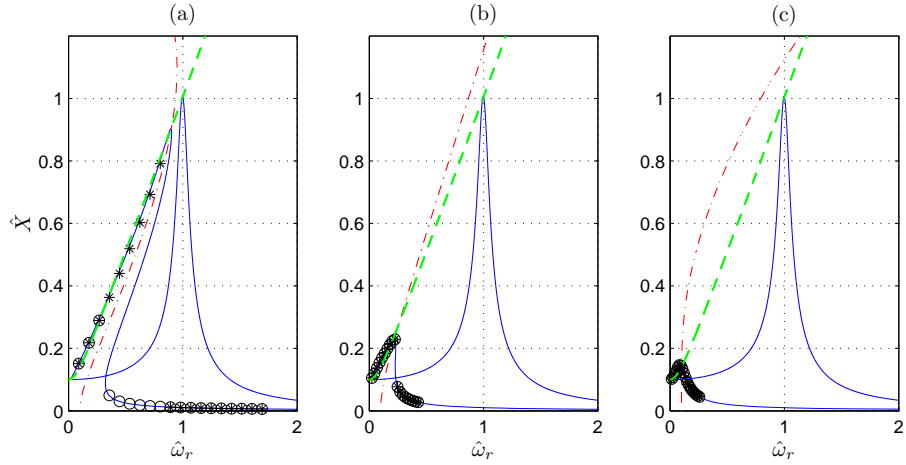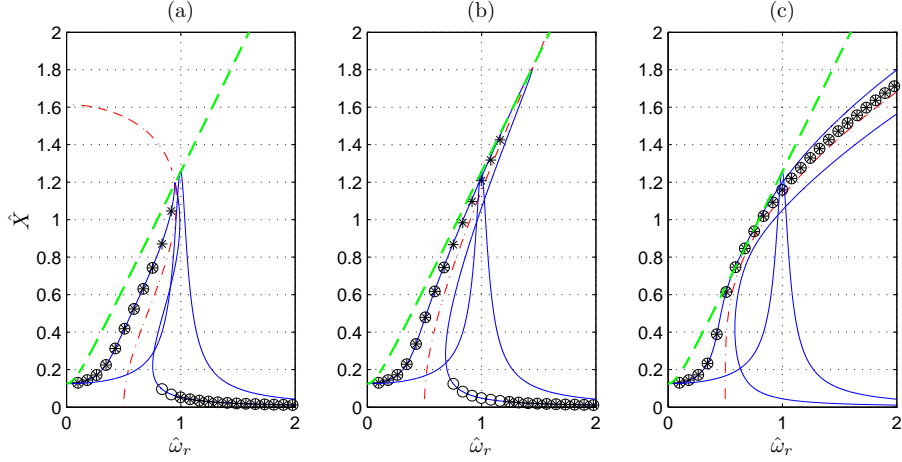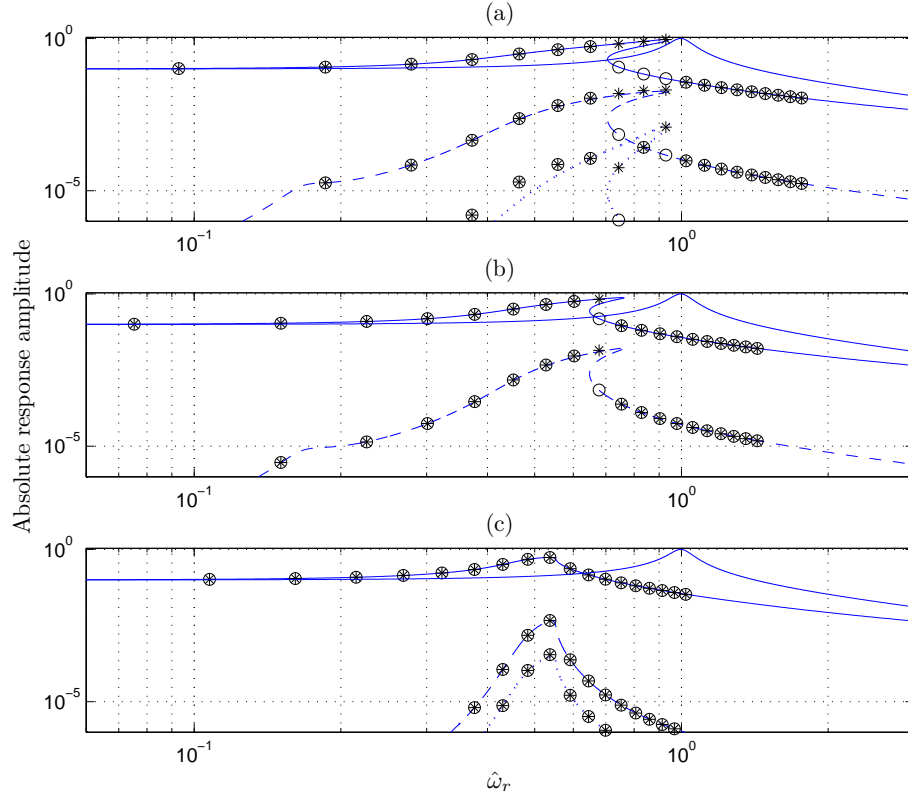

Figure 10: Predicted displacement FRF at forcing frequency for base motion excitation (solid) (a) $\hat{z}_r = 0.447$ (b) $\hat{z}_r = 0.577$ (c) $\hat{z}_r = 0.669$. Right hand peak shows response of equivalent linear system for comparison. Markers show simulation results; ($*$) denotes upwards frequency stepping, ($\circ$) denotes downwards frequency stepping. Dashed line shows limit curve, dot-dashed line shows backbone curve. $\hat{k}_e = 0.01$, $\lambda = 0.05$, $\hat{R} = 0.1$

21

Figure 11: Predicted displacement FRF at forcing frequency for base motion excitation (solid) (a) $\hat{z}_r = 0.447$ (b) $\hat{z}_r = 0.577$ (c) $\hat{z}_r = 0.669$. Right hand peak shows response of equivalent linear system for comparison. Markers show simulation results; ($*$) denotes upwards frequency stepping, ($\circ$) denotes downwards frequency stepping. $\hat{k}_e = 0.25$, $\lambda = 0.05$, $\hat{R} = 0.125$

mount properties; the backbone curve for the 5th order approximation is shown, alongside curves that modify its properties. We see that reducing $\hat{k}_e$ by 20% has some benefit at low amplitude forcing, with significant peak frequency reduction and slight peak amplitude reduction. However as excitation amplitude increases such that $1.2 > \hat{R} > 2.40\lambda$, we see that increasing $\hat{z}_r$ by 20% has a far more beneficial effect, in terms of both peak amplitude and peak frequency. We aso see that as nondimensional fundamental response amplitude exceeds 1.0, the systems begin to converge, although in all cases the peak frequency reduction is mostly lost, and amplitude is approaching levels such that our polynomial fit may now becoming invalid and assumptions of small harmonics may also be becoming invalid. So the best strategy to optimise the system will depend on the anticipated excitation levels, and if $\hat{R}/\lambda$ cannot be restricted sufficiently, a greater static displacement may have to be tolerated.

22

Figure 12: Predicted displacement amplitude FRF including harmonics for base motion excitation (a) $\hat{z}_r = 0.447$ (b) $\hat{z}_r = 0.577$ (c) $\hat{z}_r = 0.669$. Solid line shows fundamental, right hand peak shows response of equivalent linear system for comparison. Dashed line shows 3rd harmonic, dotted line shows 5th harmonic. Markers show simulation results; ($*$) denotes upwards frequency stepping, ($\circ$) denotes downwards frequency stepping. $k_e = 0.25$, $\lambda = 0.05$, $\hat{R} = 0.1$

23
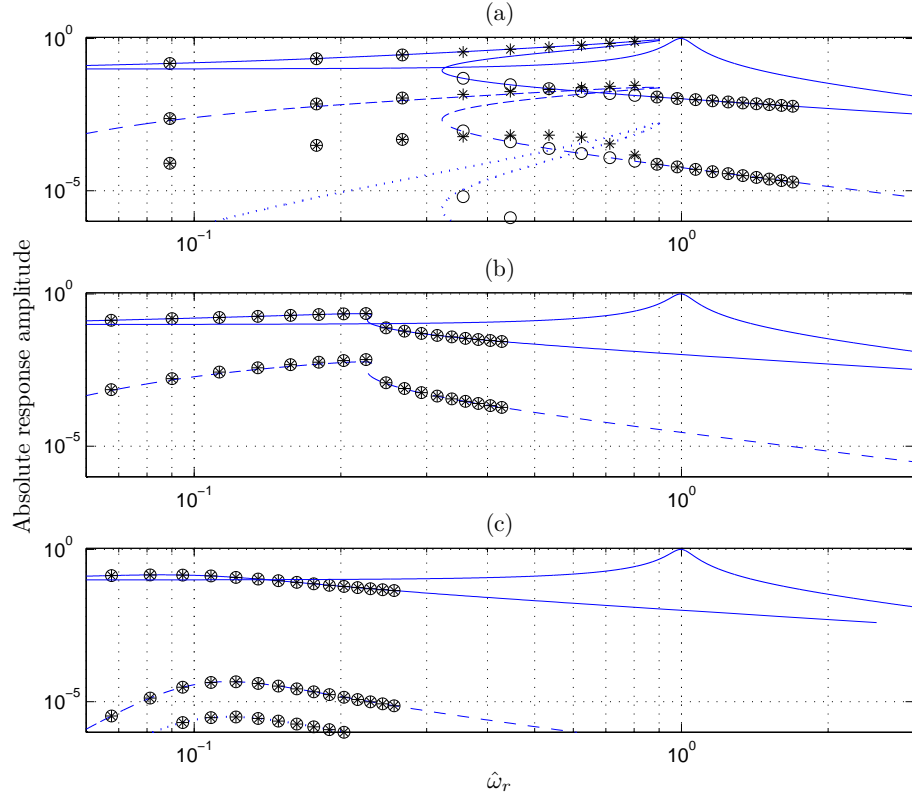
Figure 13: Predicted displacement amplitude FRF including harmonics for base motion excitation (a) $\hat{z}_r = 0.447$ (b) $\hat{z}_r = 0.577$ (c) $\hat{z}_r = 0.669$. Solid line shows fundamental, right hand peak shows response of equivalent linear system for comparison. Dashed line shows 3rd harmonic, dotted line shows 5th harmonic. Markers show simulation results; ($*$) denotes upwards frequency stepping, ($\circ$) denotes downwards frequency stepping. $k_e = 0.01$, $\lambda = 0.05$, $\hat{R} = 0.1$

24
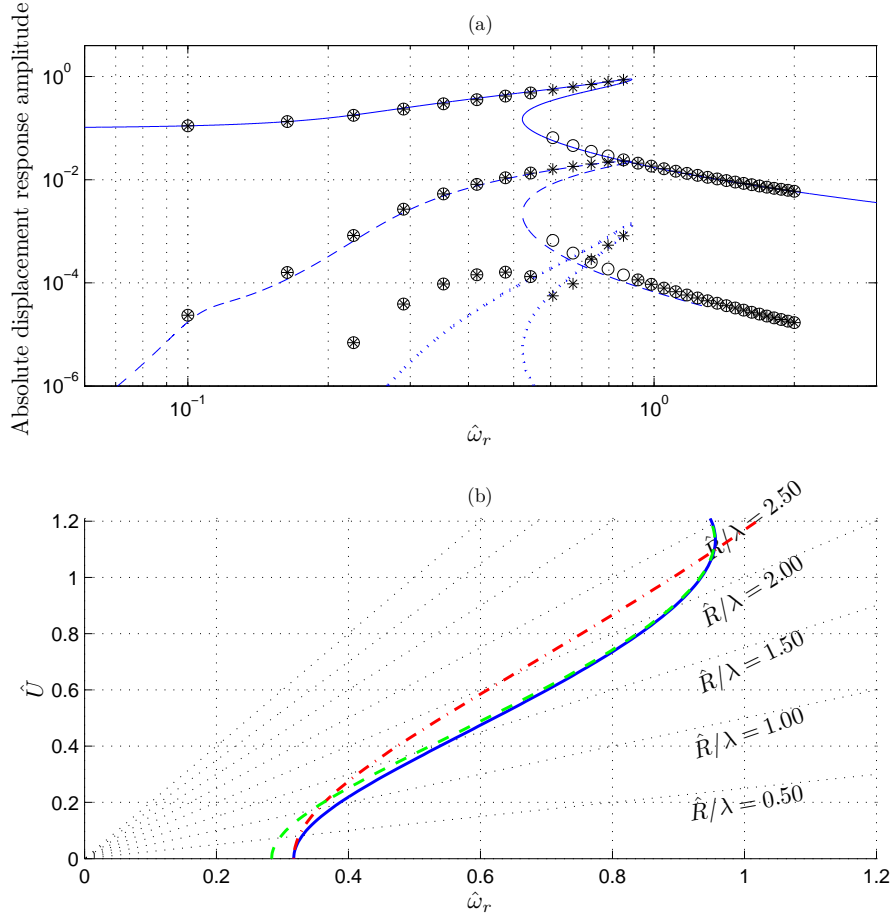
Figure 14: (a) Comparison of simulated response of nondimensional function in Fig. (5) based on Eq. (19) with Normal Form prediction based on 5th order polynomial approximation. Markers show simulation results; (∗) denotes upwards frequency stepping, (○) denotes downwards frequency stepping. $\hat{R} = 0.1$, $\lambda = 0.05$, $\hat{k}_e = 0.1005$, $\hat{z}_r = 0.4618$ (b) Example of how a limit curve map could be used to consider design changes to a given mount; Solid line shows backbone curve for above system, alongside curves for $\hat{z}_r + 20\%$ (dot-dashed) and $\hat{k}_e$-20% (dashed). Dotted lines show limit curves.

7. Conclusions

In this paper, we have provided a nondimensional analysis that shows the response of HSLDS mounts subject to harmonic excitation, relative to an equivalent linear system to demonstrate the effects of nonlinearity.

We have introduced two parameters, equilibrium stiffness and reduced stiffness range that give an accurate characterisation of HSLDS mounts' static force displacement curves, and shown that they have important effects on response. Using these parameters we have shown that a 5th order polynomial response can accurately represent much of the design space for mounts that have non-polynomial responses, and that this can give much greater realism at higher amplitudes than a Duffing response.

We have seen that at small response amplitudes the equilibrium stiffness dominates the peak response frequency of the mount, whilst at higher amplitudes the reduced stiffness range becomes important. We have shown how plotting a backbone curve on a limit curve map is a simple graphical means of understanding these effects.

We have shown that in the case of displacement response to harmonic base excitation, the HSDLS mount will always reduce both peak amplitude and peak frequency within limits of excitation amplitude. However, the base excitation case can experience sudden increases in peak response amplitude and frequency in response to small changes in system parameters, or even lead to unbounded response. The shape of the force displacement curve, as characterised by equilibrium stiffness and reduced stiffness range, is critical in predicting these effects. We provide a limiting ratio of excitation to damping below which the unbounded response cannot occur.

In the case where the mount is excited by a harmonic force signal acting upon the mass, we show that reducing the peak frequency will always lead to an increase in peak displacement response amplitude for any forcing level, meaning that there is less advantage to using the HSLDS when the amplitude response to forced excitation is of primary concern. However, this case does

not suffer from the same high parameter sensitivity and possible unbounded response that can affect the base motion case.

The analysis also provides estimates of harmonic responses of the HSLDS mount. Harmonics are small in the cases studied, suggesting that harmonics are seldom the limiting design factor for an HSLDS mount. We have shown with numerical simulation that the analysis is accurate at the fundamental frequency and third harmonics (providing assumptions are adhered to), although 5th harmonic predictions often have poor accuracy.

Overall the work provides useful insight into the design of HSLDS mounts, and demonstrates the effectiveness of the HSLDS strategy for vibration isolation.

Acknowledgements

Appendix A. Normal Forms Solutions

A Normal Form analysis is used, based on the technique desribed by Neild and Wagg [16], which provides results in terms of a transformed variable $\hat{u}$ representing the response at forcing frequency, and a transformation function $h(\hat{u})$ which contain information on harmonic responses. This method is modified for this purpose to allow the damping to be applied to harmonics as described later, which improves accuracy at certain frequencies.

Appendix A.1. Normal forms transformation

We assume either a harmonic base motion or harmonic forcing excitation, and rearrange the equation of motion Eq. (6) to:

$$\hat{z}'' + 2\lambda\hat{z}' + \hat{\omega}_n^2\hat{z} + \hat{N}_z(\hat{z}) = \mathbf{P_r}\mathbf{r} \tag{A.1}$$

where linearised natural frequency $\hat{\omega}_n^2 = \hat{k}_e$ (due to the fact that mass is unity in our nondimensionalisation), and $\hat{N}_z(\hat{z})$ contains all nonlinear stiffness terms,

hence using 5th order polynomial functions will be given by:

$$\hat{N}_z(\hat{z}) = \hat{P}(\hat{z}) - \hat{k}_e\hat{z} = k_3\hat{z}^3 + k_5\hat{z}^5 \tag{A.2}$$

Note that the damping term does not include $\hat{\omega}_n$ on account of our slightly unusual nondimensionalisation. In the right hand side of Eq. (A.1), $\mathbf{r} = \{r_p, r_m\}^T = \left\{e^{i(\hat{\Omega}\tau+\phi)}, e^{-i(\hat{\Omega}\tau+\phi)}\right\}^T$, hence defining a cosine forcing signal with forcing frequency $\hat{\Omega}$ where the time-shift ϕ has been applied so that phase does not appear in trial solutions, simplifying computations. The remaining term is the excitation vector $\mathbf{P_r} = \left[\frac{P_r}{2}, \frac{P_r}{2}\right]$, where P_r gives the amplitude and is given by:

$$P_r = \hat{\Omega}^2\hat{R} \tag{A.3}$$

in the case of base excitation with nondimensional amplitude $\hat{R}$ and

$$P_r = \hat{F} \tag{A.4}$$

in the case of forcing excitation with nondimensional amplitude $\hat{F}$.

The normal forms method seeks to find a near-identity transformation of $\hat{z}$ such that it is possible to exactly solve the transformed equation of motion:

$$\hat{u}'' + 2\lambda\hat{u}' + \hat{\omega}_n^2\hat{u} + \hat{N}_u(\hat{u}) = \mathbf{P_u}\mathbf{r} \tag{A.5}$$

where

$$\hat{u} = z - h(\hat{u}) \tag{A.6}$$

We therefore seek to choose $h(\hat{u})$ and $\hat{N}_u(\hat{u})$ to eliminate nonlinear terms, ideally so $\hat{N}_u(\hat{u}) = 0$ so that equation Eq. (A.5) is linear, although this is not usually possible. However it is generally possible to create a situation where Eq. (A.5) can be solved exactly with with a single frequency response. To assist the analysis we introduce a 'book keeping' term ϵ to indicate small terms, remembering that our assumptions of weak nonlinearity and near-identity transformation mean that:

$$h(\hat{u}) = \epsilon h(\hat{u}) \tag{A.7}$$

$$\hat{N}_u(\hat{u}) = \epsilon\hat{N}_u(\hat{u}) \tag{A.8}$$

$$\hat{N}_z(\hat{z}) = \epsilon\hat{N}_z(\hat{z}) \tag{A.9}$$

28

Note that many treatments of this method apply ϵ to the damping term as well— this is not done here which leads to improved estimation of harmonics when forcing is below resonance and forcing is light enough to ensure harmonics remain small in comparison to fundamental response even when resonant. Combining Eq. (A.1) and Eq. (A.5) to Eq. (A.9) we can obtain:

$$\mathbf{P_u r} - \mathbf{P_r r} = \epsilon \hat{N}_u(\hat{u}) - \epsilon h(\hat{u})'' - 2\epsilon\lambda h(\hat{u})' - \hat{\omega}_n^2 \epsilon h(\hat{u}) - \epsilon \hat{N}_z(\hat{u} + \epsilon h(\hat{u})) \quad \text{(A.10)}$$

The final term of this may be approximated via Taylor series expansion:

$$\epsilon \hat{N}_z(\hat{u} + \epsilon h(\hat{u})) = \epsilon \hat{N}_z(\hat{u}) + \frac{\epsilon^2 h(\hat{u})}{2}\frac{d\hat{N}_z}{d\hat{z}} + \epsilon^3 h(\hat{u})^2 \frac{d^2 \hat{N}_z}{d\hat{z}^2} \dots$$
$$= \epsilon \hat{N}_z(\hat{u}) + \mathcal{O}(\epsilon^2) \quad \text{(A.11)}$$

So making this approximation we get:

$$\mathbf{P_u r} - \mathbf{P_r r} = \epsilon \hat{N}_u(\hat{u}) - \epsilon h(\hat{u})'' - 2\epsilon\lambda h(\hat{u})' - \epsilon\hat{\omega}_n^2 h(\hat{u}) - \epsilon \hat{N}_z(\hat{u}) \quad \text{(A.12)}$$

to order ϵ^2. A natural way to achieve this is to balance the large terms and small terms of the above equation separately giving:

$$\mathbf{P_u} = \mathbf{P_z} \quad \text{(A.13)}$$

and

$$\hat{N}_u(\hat{u}) = h(\hat{u})'' + 2\lambda h(\hat{u})' + \hat{\omega}_n^2 h(\hat{u}) + \hat{N}_z(\hat{u}) \quad \text{(A.14)}$$

We now propose a propose a trial solution:

$$\hat{u} = \hat{u}_p + \hat{u}_m \quad \text{(A.15)}$$

where $\hat{u}_p = \frac{\hat{U}}{2}e^{\mathbf{i}\hat{\omega}_r \tau}$ and $\hat{u}_m = \frac{\hat{U}}{2}e^{-\mathbf{i}\hat{\omega}_r \tau}$, in effect a fundamental response that is a cosine function (recall phase shift has been applied to the forcing function). Firstly we substitute this solution into $\hat{N}_z(\hat{u})$ to see what terms are generated. For illustration, let us suppose that $\hat{N}_z$ is just a Duffing/cubic type nonlinearity:

$$\hat{N}_z(\hat{u}) = k_3 \hat{u}^3 = k_3 \hat{u}_p^3 + k_3 \hat{u}_m^3 + 3k_3 \hat{u}_p^2 \hat{u}_m + 3k_3 \hat{u}_p \hat{u}_m^2 \quad \text{(A.16)}$$

which may be written:

$$\hat{N}_z(\hat{u}) = \begin{bmatrix} k_3 & k_3 & 3k_3 & 3k_3 \end{bmatrix} \begin{Bmatrix} \hat{u}_p^3 \hat{u}_m^0 \\ \hat{u}_p^0 \hat{u}_m^3 \\ \hat{u}_p^2 \hat{u}_m^1 \\ \hat{u}_p^1 \hat{u}_m^2 \end{Bmatrix} \tag{A.17}$$

It can be seen that this can be generalised for any polynomial nonlinearities to the form:

$$\hat{N}_z(\hat{u}) = \hat{\mathbf{N}}_\mathbf{z} \hat{\mathbf{u}}^* \tag{A.18}$$

where $\hat{\mathbf{N}}_\mathbf{z}$ is a row vector of coefficients and $\hat{\mathbf{u}}^*$ is a column vector where the elements all have the form:

$$\hat{u}_{i,j}^* = \hat{u}_p^i \hat{u}_m^j \tag{A.19}$$

We specify that $h(\hat{u})$ and $\hat{N}_u(\hat{u})$ have a similar form:

$$\hat{N}_u(\hat{u}) = \hat{\mathbf{N}}_\mathbf{u} \hat{\mathbf{u}}^* \tag{A.20}$$

$$h(\hat{u}) = \mathbf{h} \hat{\mathbf{u}}^* \tag{A.21}$$

For Eq. (A.14) we require $h(\hat{u})'$ and $h(\hat{u})''$, so we note that for any element $\hat{u}_{i,j}^*$ of $\hat{\mathbf{u}}*$:

$$\hat{u}_{i,j}^{*\prime} = \mathbf{i}\,(i-j)\,\hat{\omega}_r \hat{u}_{i,j}^* = \mathbf{i}\hat{\omega}_{i,j}\hat{u}_{i,j}^* \tag{A.22}$$

$$\hat{u}_{i,j}^{*\prime\prime} = -\,(i-j)^2\,\hat{\omega}_r^2 \hat{u}_{i,j}^* = -\hat{\omega}_{i,j}^2 \hat{u}_{i,j}^* \tag{A.23}$$

such that

$$h(\hat{u})' = \mathbf{i}\mathbf{h}\hat{\boldsymbol{\omega}}\hat{\mathbf{u}}^* \tag{A.24}$$

$$h(\hat{u})'' = -\mathbf{h}\hat{\boldsymbol{\omega}}^\mathbf{2}\hat{\mathbf{u}}^* \tag{A.25}$$

where $\hat{\boldsymbol{\omega}}$ is a diagonal matrix of $\hat{\omega}_{i,j}$ terms and $\hat{\boldsymbol{\omega}}^\mathbf{2}$ is similar with $\hat{\omega}_{i,j}^2$ terms. Putting all of this into Eq. (A.14) gives:

$$\left(-\mathbf{h}\hat{\boldsymbol{\omega}}^\mathbf{2} + 2\lambda\mathbf{i}\mathbf{h}\hat{\boldsymbol{\omega}} + \hat{\omega}_n^2\mathbf{h} - \hat{\mathbf{N}}_\mathbf{u} + \hat{\mathbf{N}}_\mathbf{z}\right)\hat{\mathbf{u}}^* = 0 \tag{A.26}$$

which for solutions requires that:

$$\mathbf{h}\hat{\boldsymbol{\omega}}^\mathbf{2} - \hat{\omega}_n^2\mathbf{h} - 2\lambda\mathbf{i}\mathbf{h}\hat{\boldsymbol{\omega}} = \hat{\mathbf{N}}_\mathbf{z} - \hat{\mathbf{N}}_\mathbf{u} \tag{A.27}$$

because each term in $\hat{\mathbf{u}}^*$ has a unique i and j representing a different time varying function so cannot be set to zero (unless $\hat{U} = 0$, which is trivial). We solve this by solving each term individually:

$$\left((i-j)^2\,\hat{\omega}_r^2 - \hat{\omega}_n^2 - 2\lambda\mathbf{i}\,(i-j)\,\hat{\omega}_r\right) h_{i,j} = \hat{N}_{z_{i,j}} - \hat{N}_{u_{i,j}} \tag{A.28}$$

By default, we seek to eliminate nonlinear terms from Eq. (A.5), so we set $\hat{N}_{u_{i,j}}$ to zero and write:

$$h_{i,j} = \frac{\hat{N}_{z_{i,j}}}{(i-j)^2\,\hat{\omega}_r^2 - \hat{\omega}_n^2 - 2\lambda\mathbf{i}\,(i-j)\,\hat{\omega}_r} \tag{A.29}$$

However, if the denominator in this equation is small, $h_{i,j}$ would become large and violate our assumption of near-identity transformation. In these cases we must set $h_{i,j}$ to zero and let

$$\hat{N}_{z_{i,j}} = \hat{N}_{u_{i,j}} \tag{A.30}$$

This is known as a resonant term. If we assume response frequency is similar to forcing frequency and that the forcing frequency is near resonance, it is evident from Eq. (A.29) that a resonant term will occur whenever $|i - j| = 1$, because this will cancel all terms except the damping term, which is assumed to be light. Note that at different response frequencies, different terms become resonant. For example, if response frequency is at $1/3$ of the natural frequency, terms will become resonant when $|i - j| = 3$ (i.e. the third harmonic is resonant). However, we find that even when resonant, harmonic terms seldom become sufficiently large to be treated as the primary response in the light excitation cases considered.

Appendix A.2. Solving resonant dynamics equation to obtain $\hat{U}$

To show how Normal forms can now be used to solve the transformed equation of motion Eq. (A.5), refer to the example of a cubic power term, with the expansion of the assumed solution. The third and fourth terms are both

resonant in this case, so $\hat{N}_u$ becomes:

$$\hat{N}_u(\hat{u}) = \begin{bmatrix} 0 & 0 & 3k_3 & 3k_3 \end{bmatrix} \begin{Bmatrix} \hat{u}_p^3\hat{u}_m^0 \\ \hat{u}_p^0\hat{u}_m^3 \\ \hat{u}_p^2\hat{u}_m^1 \\ \hat{u}_p^1\hat{u}_m^2 \end{Bmatrix}$$

$$= \frac{3k_3\hat{U}^3}{4}\cos(\hat{\omega}_r\tau) \quad \text{(A.31)}$$

where the cosine term has been derived using De Moivre's theorem. It can be seen that each power n term will contribute in a similar manner. We can sum all these contributions along with the linearised stiffness $\hat{\omega}_n^2 = \hat{k}_e$ in an amplitude dependant stiffness function $K(\hat{U})$, which can be written:

$$K(\hat{U}) = \hat{k}_e + \sum_n k_n \begin{pmatrix} p \\ n \end{pmatrix} \frac{\hat{U}^{n-1}}{2^{n-1}} \quad \text{(A.32)}$$

where $p = n/2$ for even n, $p = (n-1)/2$ for odd n. For a 5th order system we obtain:

$$K(\hat{U}) = \hat{k}_e + \frac{3k_3\hat{U}^2}{4} + \frac{10k_5\hat{U}^4}{16} \quad \text{(A.33)}$$

Substituting this and the assumed solution into the transformed equation of motion Eq. (A.5), and changing the complex notation to trigonometric terms gives:

$$-\hat{\omega}_r^2\hat{U}\cos(\hat{\omega}_r\tau) - 2\hat{U}\hat{\omega}_r\lambda\sin(\hat{\omega}_r\tau) + K(\hat{U})\hat{U}\cos(\hat{\omega}_r\tau)$$

$$= \hat{P}_u\cos(\hat{\Omega}\tau + \phi) \quad \text{(A.34)}$$

We substitute our assumption that $\hat{\omega}_r = \hat{\Omega}$ and use a trigonometric identity to expand the right hand term to get:

$$-\hat{\omega}_r^2\hat{U}\cos(\hat{\omega}_r\tau) - 2\hat{U}\hat{\omega}_r\lambda\sin(\hat{\omega}_r\tau) + K(\hat{U})\hat{U}\cos(\hat{\omega}_r\tau)$$

$$= \hat{P}_u\left[\cos(\hat{\omega}_r\tau)\cos(\phi) + \sin(\hat{\omega}_r\tau)\sin(\phi)\right] \quad \text{(A.35)}$$

Matching the $\cos(\hat{\omega}_r)$ and $\sin(\hat{\omega}_r)$ terms gives the following two equations:

$$-\hat{\omega}_r^2\hat{U} + K(\hat{U})\hat{U} = \hat{P}_u\cos(\phi) \quad \text{(A.36)}$$

$$-2\hat{U}\hat{\omega}_r\lambda = -\hat{P}_u\sin(\phi) \quad \text{(A.37)}$$

We square and add equations Eq. (A.36) and Eq. (A.37) to eliminate ϕ:

$$\hat{\omega}_r^4 \hat{U}^2 + 2\hat{\omega}_r^2 \hat{U}^2 \left[2\lambda^2 - K(\hat{U}) \right] + K(\hat{U})^2 \hat{U}^2 - \hat{P}_u^2 = 0 \qquad \text{(A.38)}$$

We substitute Eq. (A.3) to get the response equation for base excitation:

$$\hat{\omega}_r^4 (\hat{U}^2 - \hat{R}^2) + 2\hat{\omega}_r^2 \hat{U}^2 \left[2\lambda^2 - K(\hat{U}) \right] + K(\hat{U})^2 \hat{U}^2 = 0 \qquad \text{(A.39)}$$

and similarly we substitute Eq. (A.4) to get the response equation for forced excitation:

$$\hat{\omega}_r^4 \hat{U}^2 + 2\hat{\omega}_r^2 \hat{U}^2 \left[2\lambda^2 - K(\hat{U}) \right] + K(\hat{U})^2 \hat{U}^2 - \hat{F}^2 = 0 \qquad \text{(A.40)}$$

These equations are quadratic in $\hat{\omega}_r^2$ so may be solved for $\hat{\omega}_r^2$ with any trial value of $\hat{U}$, obtaining up to 2 real solutions. Phase may then be determined by using either Eq. (A.36) or Eq. (A.37).

Appendix A.3. Estimation of Harmonics

We now consider non-resonant terms, which become part of the transformation $h(\hat{u})$ and dictate the harmonic responses of the system. We notice from the expansion of the Duffing term Eq. (A.17) that there are two non-resonant terms $k_3 \hat{u}_0^3$ and $k_3 \hat{u}_3^0$, where the indices i and j are swapped. For illustration consider the combined contribution of the non-resonant terms from the Duffing equation, calculated using equation Eq. (A.29):

$$h_{3,0} + h_{0,3} =$$

$$\frac{k_3 (\hat{u}_p^3 \hat{u}_m^0)}{(3-0)^2 \hat{\omega}_r^2 - \hat{\omega}_n^2 - \mathbf{i}(3-0)\hat{\omega}_r(2\lambda)} + \frac{k_3 (\hat{u}_p^0 \hat{u}_m^3)}{(0-3)^2 \hat{\omega}_r^2 - \hat{\omega}_n^2 - \mathbf{i}(0-3)\hat{\omega}_r(2\lambda)}$$

$$= \frac{3 k_3 (\hat{U}^3/4)}{(9\hat{\omega}_r^2 - \hat{\omega}_n^2)^2 + (6\hat{\omega}_r\lambda)^2} \left((9\hat{\omega}_r^2 - \hat{\omega}_n^2) \cos(3\hat{\omega}_r\tau) + \mathbf{i}(6\hat{\omega}_r\lambda) \sin(3\hat{\omega}_r\tau) \right) \quad \text{(A.41)}$$

which is a sinusoidal signal that can be resolved into a phase and magnitude. The magnitude is:

$$h_3 = \frac{k_3 (\hat{U}^3/4)}{\sqrt{(9\hat{\omega}_r^2 - \hat{\omega}_n^2)^2 + (6\hat{\omega}_r\lambda)^2}} \qquad \text{(A.42)}$$

For a 5th order polynomial system, we apply a similar procedure to obtain the following magnitudes of the 3rd and 5th harmonics:

$$h_3(\hat{u}) = \left(\frac{k_3 \hat{U}^3}{4} + \frac{5k_5 \hat{U}^5}{16} \right) \frac{1}{\sqrt{(9\hat{\omega}_r^2 - \hat{\omega}_n^2)^2 + (6\hat{\omega}_r \lambda)^2}} \qquad (A.43)$$

and

$$h_5(\hat{u}) = \frac{k_5 \hat{U}^5}{16} \frac{1}{\sqrt{(25\hat{\omega}_r^2 - \hat{\omega}_n^2)^2 + (10\hat{\omega}_r \lambda)^2}} \qquad (A.44)$$

Appendix A.4. Backbone and Limit Curves

If we consider an undamped and unexcited solution, Eq. (A.37) disappears, and Eq. (A.36) alone defines solutions, becoming:

$$\hat{\omega}_r = \sqrt{K(\hat{U})} \qquad (A.45)$$

Recalling that light damping has very little effect on response frequencies, we see that all peak responses for lightly damped systems lie somewhere on the line defined by this equation, which is known as the backbone curve and defines the amplitude dependant natural frequency. (Note that an HSLDS mount is intended to perform at frequencies above resonance, where response is dominated by damping. Therefore a lightly damped mount is desirable.) We also note that backbone curves are identical for both base motion and forced excitation. Returning to an excited and damped system, we use the intuition that at a natural frequency $\phi = \frac{\pi}{2}$ and that the excitation is purely resisted by damping, Eq. (A.36) disappears and Eq. (A.37) defines peak response. Therefore:

$$2\hat{\Omega}\lambda\hat{U} = P_r \Rightarrow \hat{U} = \frac{P_r}{2\lambda\hat{\Omega}} \qquad (A.46)$$

This defines the limit curve for a given system. The point where a limit curve and backbone curve intersect on a frequency/amplitude graph defines peak response for the system concerned, for a given excitation level. Note that $K(\hat{U})$ does not affect the limit curves, therefore limit curves are common to all systems with equal damping and forcing, regardless of the stiffness nonlinearities that are present. If we substitute Eq. (A.3) into Eq. (A.46) we find that the limit
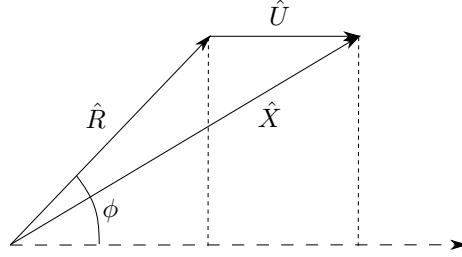
Figure A.15: Phase diagram providing geometrical basis of $\hat{X}$ calculation.

curve specifically for base excitation is:

$$\hat{U} = \frac{\hat{\Omega}\hat{R}}{2\lambda} \tag{A.47}$$

however if we substitute Eq. (A.4) into Eq. (A.46) we find that the limit curve for forced excitation is:

$$\hat{U} = \frac{\hat{F}}{2\lambda\hat{\Omega}} \tag{A.48}$$

Therefore the two types of forcing have very different limit trends; base excitation has a limit amplitude proportional to peak excitation frequency, whereas forced excitation has a limit amplitude that is inversely proportional to peak excitation frequency.

Appendix A.5. Absolute response

For base excitation it is often necessary to know the absolute displacement response in addition to the relative displacement response (the two responses are identical for forced excitation). We calculate $\hat{X}$, the amplitude of absolute response at the forcing frequency, using equation Eq. (1) and the phase diagram in Fig. (A.15) to be:

$$\hat{X} = \sqrt{(\hat{U} + \hat{R}\cos(\phi))^2 + (\hat{R}\sin(\phi))^2} \tag{A.49}$$

References

[1] D. J. Mead, Passive Vibration Control, John Wiley and Sons, 1999.

[2] A. Carrella, Passive Vibration Isolators with High-Static-Low-Dynamic-Stiffness, VDM Verlag Dr. Muller, 2010.

[3] R. A. Ibrahim, Recent advances in nonlinear passive vibration isolators, Journal of Sound and Vibration 314 (3-5) (2008) 371 – 452.

[4] J. Winterflood, D. G. Blair, B. Slagmolen, High performance vibration isolation using springs in euler column buckling mode, Physics Letters A 300 (2-3) (2002) 122–130.

[5] L. N. Virgin, R. B. Davis, Vibration isolation using buckled struts, Journal of Sound and Vibration 260 (5) (2003) 965–973.

[6] R. H. Plaut, J. E. Sidbury, L. N. Virgin, Analysis of buckled and pre-bent fixed-end columns used as vibration isolators, Journal of Sound and Vibration 283 (3-5) (2005) 1216–1228.

[7] L. N. Virgin, S. T. Santillan, R. H. Plaut, Vibration isolation using extreme geometric nonlinearity, Journal of Sound and Vibration 315 (3) (2008) 721–731.

[8] S. T. Santillan, Analysis of the elastica with applications to vibration isolation, Ph.D. thesis, Department of Mechanical Engineering and Materials Science, Duke University (2007).

[9] R. DeSalvo, Passive, nonlinear, mechanical structures for seismic attenuation, Journal of Computational and Nonlinear Dynamics 2 (4) (2007) 290–298.

[10] A. Carrella, M. J. Brennan, T. P. Waters, Static analysis of a passive vibration isolator with quasi-zero-stiffness characteristic, Journal of Sound and Vibration 301 (301) (2007) 678 – 689.

[11] A. Carrella, M. J. Brennan, T. P. Waters, V. Lopes Jr., Force and displacement transmissibility of a nonlinear isolator with high-static-low-dynamic-stiffness, International Journal of Mechanical Sciences 55 (1) (2012) 22 – 29.

[12] I. Kovacic, M. J. Brennan, T. P. Waters, A study of a nonlinear vibration isolator with a quasi-zero stiffness characteristic, Journal of Sound and Vibration 315 (3) (2008) 700 – 711.

[13] N. Zhou, K. Liu, A tunable high-static low-dynamic stiffness vibration isolator, Journal of Sound and Vibration 329 (9) (2010) 1254 – 1273.

[14] W. S. Robertson, M. R. F. Kidner, B. S. Cazzolato, A. C. Zander, Theoretical design parameters for a quasi-zero stiffness magnetic spring for vibration isolation, Journal of Sound and Vibration 1-2 (2009) 88–103.

[15] T. D. Le, K. K. Ahn, A vibration isolation system in low frequency excitation region using negative stiffness structure for vehicle seat, Journal of Sound and Vibration 330 (26) (2011) 6311–6335.

[16] S. A. Neild, D. J. Wagg, Applying the method of normal forms to second-order nonlinear vibration problems, Proc. R. Soc. A 467 (2128) (2010) 1141 – 1163.

[17] S. A. Neild, Approximate methods for analysing nonlinear structures, in: L. N. Virgin, D. J. Wagg (Eds.), Exploiting Nonlinear Behaviour in Structural Dynamics, Springer, 2012, pp. 53 – 109.

[18] D. J. Wagg, S. A. Neild, Nonlinear Vibration with Control, Springer, 2009.

[19] A. H. Nayfeh, D. T. Mook, Nonlinear Oscillations, John Wiley and Sons, 1979.

List of Figures